Springer

Dear Author

Here are the proofs of your article.

- You can submit your corrections **online,** via **e-mail** or by **fax**.
- For **online** submission please insert your corrections in the online correction form. Always indicate the line number to which the correction refers.
- You can also insert your corrections in the proof PDF and **email** the annotated PDF.
- For **fax** submission, please ensure that your corrections are clearly legible. Use a fine black pen and write the correction in the margin, not too close to the edge of the page.
- Remember to note the **journal title**, **article number**, and **your name** when sending your response via e-mail or fax.
- **Check** the metadata sheet to make sure that the header information, especially author names and the corresponding affiliations are correctly shown.
- **Check** the questions that may have arisen during copy editing and insert your answers/corrections.
- **Check** that the text is complete and that all figures, tables and their legends are included. Also check the accuracy of special characters, equations, and electronic supplementary material if applicable. If necessary refer to the *Edited manuscript*.
- The publication of inaccurate data such as dosages and units can have serious consequences. Please take particular care that all such details are correct.
- Please **do not** make changes that involve only matters of style. We have generally introduced forms that follow the journal's style.
- Substantial changes in content, e.g., new results, corrected values, title and authorship are not allowed without the approval of the responsible editor. In such a case, please contact the Editorial Office and return his/her consent together with the proof.
- If we do not receive your corrections **within 48 hours**, we will send you a reminder.
- Your article will be published **Online First** approximately one week after receipt of your corrected proofs. This is the **official first publication** citable with the DOI. **Further changes are, therefore, not possible.**
- The **printed version** will follow in a forthcoming issue.

Please note

After online publication, subscribers (personal/institutional) to this journal will have access to the complete article via the DOI using the URL:

`http://dx.doi.org/10.1007/s10346-014-0498-5`

If you would like to know when your article has been published online, take advantage of our free alert service. For registration and further information, go to: http://www.link.springer.com.

Due to the electronic nature of the procedure, the manuscript and the original figures will only be returned to you on special request. When you return your corrections, please inform us, if you would like to have these documents returned.

AUTHOR'S PROOF!

Metadata of the article that will be visualized in OnlineFirst

1	Article Title	**Geomechanical assessment of the Corvara earthflow through numerical modelling and inverse analysis**	
2	Article Sub- Title		
3	Article Copyright - Year	**Springer-Verlag Berlin Heidelberg 2014 (This will be the copyright line in the final PDF)**	
4	Journal Name	Landslides	
5	Corresponding Author	Family Name	**Borgatti**
6		Particle	
7		Given Name	**L.**
8		Suffix	
9		Organization	University of Bologna
10		Division	Department of Civil, Chemical, Environmental and Materials Engineering DICAM~~, ALMA MATER STUDIORUM~~
11		Address	Viale Risorgimento 2, Bologna 40136, Italy
12		e-mail	lisa.borgatti@unibo.it
13	Author	Family Name	**Schädler**
14		Particle	
15		Given Name	**W.**
16		Suffix	
17		Organization	WPW Geoconsult Südwest GmbH
18		Division	
19		Address	Erzbergerstraße 19, Mannheim 68165, Germany
20		e-mail	
21	Author	Family Name	**Corsini**
22		Particle	
23		Given Name	**A.**
24		Suffix	
25		Organization	University of Modena and Reggio Emilia
26		Division	Department of Chemical and Geological Sciences DSCG
27		Address	Largo Sant’Eufemia 19, Modena 41121, Italy
28		e-mail	

29	Author	Family Name	**Meier**
30		Particle	
31		Given Name	**J.**
32		Suffix	
33		Organization	Gruner AG
34		Division	
35		Address	Gellertstrasse 55, Basel 4020, Switzerland
36		e-mail	
37	Author	Family Name	**Ronchetti**
38		Particle	
39		Given Name	**F.**
40		Suffix	
41		Organization	University of Modena and Reggio Emilia
42		Division	Department of Chemical and Geological Sciences DSCG
43		Address	Largo Sant'Eufemia 19, Modena 41121, Italy
44		e-mail	
45	Author	Family Name	**Schanz**
46		Particle	
47		Given Name	**T.**
48		Suffix	
49		Organization	Ruhr-Universität Bochum
50		Division	Foundation Engineering, Soil and Rock Mechanics, Faculty of Civil and Environmental Engineering
51		Address	Building IC 5, Universitätsstrasse 150, Bochum 44780, Germany
52		e-mail	

53	Schedule	Received	30 April 2013
54		Revised	
55		Accepted	30 May 2014

56 Abstract

This research proposes a conceptual approach for analysis and numerical modelling of the hydromechanical behaviour of large landslides, applied to one of the source areas of the Corvara earthflow (Dolomites, Italy). The approach consists of two steps: forward calculation and inverse analysis. For the forward calculations, the geological model of the slope considering several shear zones delimitating landslide units was developed, based on a detailed dataset of field investigation and monitoring data. A viscoplastic constitutive model was used to describe the time-dependent material behaviour, i.e. the creep, of the shear zones. The transient distribution of pore water pressure in the slope was considered by means of an additional purely hydrogeological model. These results were used as averaged hydraulic boundary conditions in the calculation of stress and deformation fields with the continuum finite element method (FEM). The numerical model was then calibrated against ground surface displacement rates measured by D-GPS, by iteratively varying the material parameters of the shear zones. For this task, an inverse analysis concept was applied, based on statistical analyses and an evolutionary optimisation algorithm. The inverse modelling strategy was further applied to gather statistical information on model behaviour, on the sensitivity of model parameters and on the quality of the obtained calibration. Results show that the calibrated model was able to appropriately simulate the displacement field of the earthflow and allow the requirements, difficulties and problems, as well as the advantages and benefits of the proposed numerical modelling concept to be highlighted.

57	Keywords separated by ' - '	Finite element method - Numerical modelling - Corvara earthflow - Dolomites - Italy
58	Foot note information	

Landslides
DOI 10.1007/s10346-014-0498-5
Received: 30 April 2013
Accepted: 30 May 2014

W. Schädler · L. Borgatti · A. Corsini · J. Meier · F. Ronchetti · T. Schanz

Geomechanical assessment of the Corvara earthflow through numerical modelling and inverse analysis

Abstract This research proposes a conceptual approach for analysis and numerical modelling of the hydromechanical behaviour of large landslides, applied to one of the source areas of the Corvara earthflow (Dolomites, Italy). The approach consists of two steps: forward calculation and inverse analysis. For the forward calculations, the geological model of the slope considering several shear zones delimitating landslide units was developed, based on a detailed dataset of field investigation and monitoring data. A viscoplastic constitutive model was used to describe the time-dependent material behaviour, i.e. the creep, of the shear zones. The transient distribution of pore water pressure in the slope was considered by means of an additional purely hydrogeological model. These results were used as averaged hydraulic boundary conditions in the calculation of stress and deformation fields with the continuum finite element method (FEM). The numerical model was then calibrated against ground surface displacement rates measured by D-GPS, by iteratively varying the material parameters of the shear zones. For this task, an inverse analysis concept was applied, based on statistical analyses and an evolutionary optimisation algorithm. The inverse modelling strategy was further applied to gather statistical information on model behaviour, on the sensitivity of model parameters and on the quality of the obtained calibration. Results show that the calibrated model was able to appropriately simulate the displacement field of the earthflow and allow the requirements, difficulties and problems, as well as the advantages and benefits of the proposed numerical modelling concept to be highlighted.

Keywords Finite element method · Numerical modelling · Corvara earthflow · Dolomites · Italy

Introduction

In Italy, a number of large-scale and deep-seated complex landslides, including earthflows, affect the Alps and the Apennines (Guzzetti et al. 1994; Trigila et al. 2010). They can be up to 50 m deep and can cover several square kilometres. In the affected regions, this represents a major socio-economic problem, as landslides may cause continuous damage to infrastructures and, in several cases, they pose a potential threat to settlements.

Since few decades, numerical modelling has been applied to earthflows by various authors using different approaches, with the aim of better understanding landslide evolution (Picarelli et al. 1995; Angeli et al. 1996a, b, 1998; Vulliet and Bonnard 1996; van Asch et al. 2007; Comegna et al. 2007). In some case, the objective of the numerical modelling was to assist the design of effective technical countermeasures (Borgatti et al. 2007a; Marcato et al. 2009, 2012).

A manual trial-and-error procedure is often adopted to calibrate the numerical slope model against observed displacements. Alongside this approach, which is strongly based on expert knowledge, the application of inverse analyses for the calibration of numerical models is an appropriate concept for the identification of parameters that cannot be easily determined directly from laboratory experiments (Hvorslev 1949). Inverse analysis is widely used in many engineering fields such as hydraulics, damage analysis and structural dynamics. A variety of different optimisation schemes and algorithms are available from literature. In recent years, due to the availability of faster computer hardware, inverse parameter identification strategies and optimisation procedures have been more and more frequently used also in engineering geology and geomechanics by many authors (Gens et al. 1996; Ledesma et al. 1996a, b; Zhang et al. 2003; Calvello and Finno 2004; Malecot et al. 2004; Feng et al. 2006; Finsterle 2006; Meier et al. 2006; Levasseur et al. 2008; Meier 2008; Meier et al. 2008).

In this paper, a method for modelling the hydromechanical behaviour of large landslides is presented and applied to a source area of the Corvara earthflow in the Dolomites, Italy. This case study is relevant, as an acceleration of the landslide could determine the involvement of a part of the village, the damming of the side flank streams and the disruption of the national road running on the accumulation area.

The method consists of two parts: forward calculations and inverse analysis. In order to perform forward calculations using a continuum mechanical approach with the finite element method, different model components have to be implemented. The geological model describes the source area, and an adequate constitutive model takes into consideration weight, strength and stiffness of units and layers. In particular, a creep model describes the time-dependent behaviour of the material forming the shear zones. Additionally, a hydrogeological model describing the transient distribution of pore water pressures is used to approximate the hydraulic boundary conditions. In order to derive the parameters which yield a good simulation of reality, the finite element (FE) model is calibrated against displacement rates measured in the field, by iteratively varying the material parameters of the shear zones. For this task, the inverse parameter identification technique of Schanz et al. (2006), Schanz and Meier (2008) and Meier et al. (2008) is applied. The technique is based on statistical analyses and appropriate optimisation algorithms, which have been adapted and tested especially for geotechnical applications. Based on the Corvara case study, the requirements, difficulties and problems as well as the advantages and benefits of the proposed numerical modelling concept are highlighted.

The Corvara landslide

Setting of the landslide area

Located in a renowned tourist area in the Dolomites of Italy, the Corvara landslide (Fig. 1) was selected for this study on the basis of its socio-economic relevance and for the availability of an extensive dataset of field investigation and monitoring data.

The landslide area extends from Corvara in Badiato Pralongià, from about 1,600 to 2,100 m a.s.l. The landslide can be described as an active slow-moving earthflow with an estimated volume of 30 million m^3. It damages a national road and a set of facilities

Fig. 1 Location and overview of the Corvara earthflow

including ski infrastructures, electricity lines and a golf course. In the worst-case scenario, the landslide might accelerate and affect some buildings located at its toe and possibly endanger downstream settlements by damming the torrents running at its flanks. For this reason, geological, geomorphologic and geotechnical analyses of the landslide have been carried out since 1996 with the support of the autonomous province of Bolzano—South Tyrol, together with the Corvara municipality (Corsini et al. 2001; Soldati et al. 2004; Corsini et al. 2005; Panizza et al. 2006; Borgatti et al. 2007b; Borgatti and Soldati 2010).

Bedrock of the landslide site is mostly composed of Triassic flysch-type rock masses, La Valle and San Cassiano units, which consist of an alternation of volcano–clastic sandstones, marly limestones and clay shales. The ratio of hard to soft rocks varies from 1 to more than 2 (Corsini et al. 2005). Bedrock forms a monocline dipping upslope at about 30° of inclination, and shows three to four major tectonic joint sets generated during the Alpine orogen (Corsini 2000). The overall geomorphologic setting of the slope is primarily controlled by the attitude of bedding and

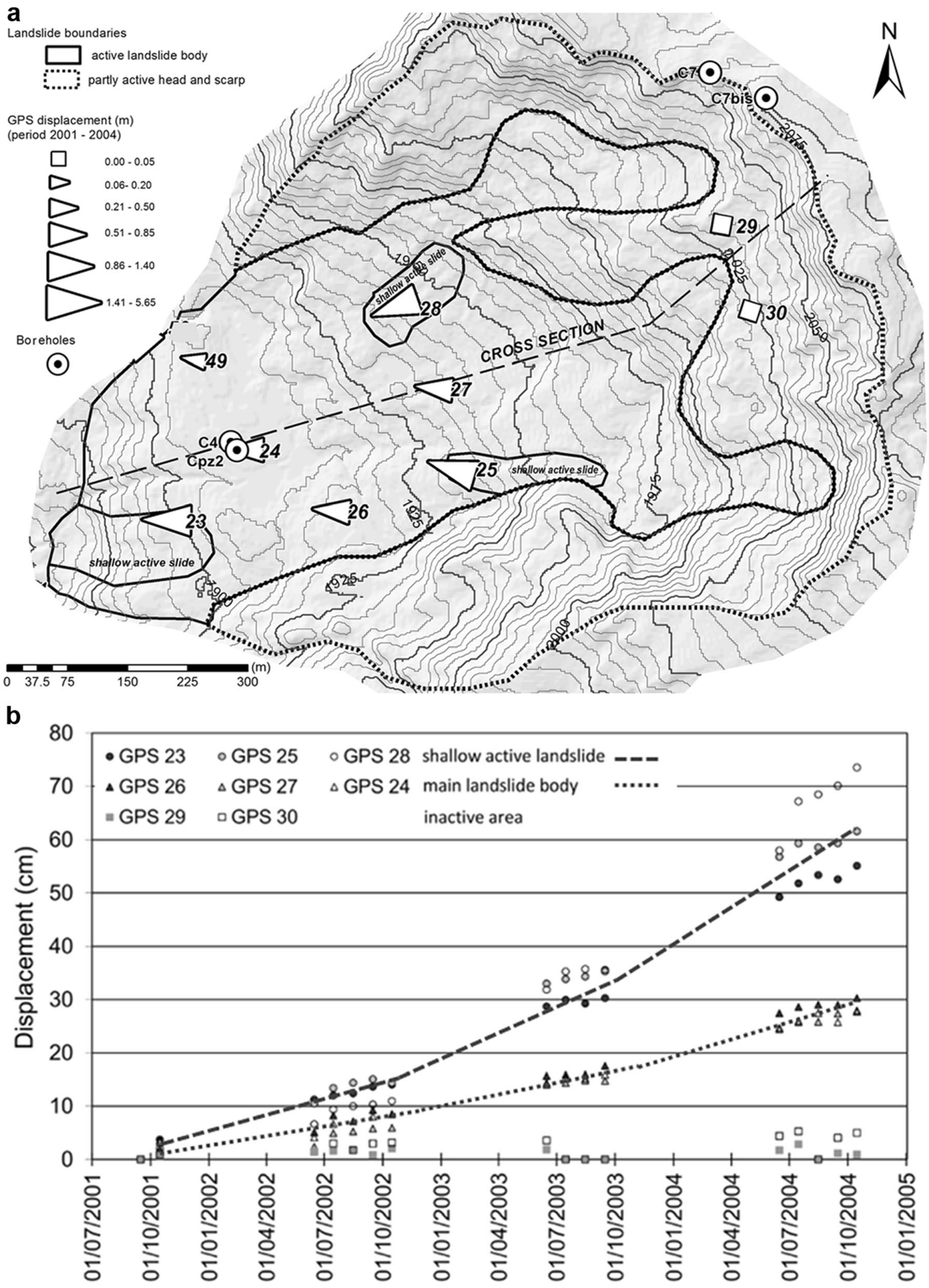

Fig. 2 Displacement vectors (**a**) and displacements (**b**) measured in source area S3 between 2001 and 2004 (GPS data from Panizza et al. 2006). Benchmark 49 was measured starting from 2003; vector has been scaled up respectively. Location of boreholes and of cross section of Fig. 5 is also reported (**a**)

joints and, secondarily, by the action of Pleistocene glaciers and of Holocene weathering and mass wasting processes (Corsini et al. 1999; Corsini 2000).

At present, in the Corvara landslide, distinct source (S), track (T) and accumulation (A) areas can be outlined. The source area itself can be subdivided into four sectors (S1, S2, S3 and S4 in

Fig. 1). Observations made on borehole cores, radiocarbon data and historical archives point to a long-term landslide evolution characterised by periods of increased activity during which the main scarp probably retrogressed, the accumulation zone grew and the earthflow foot advanced down the valley (Corsini et al. 2005; Panizza et al. 2006).

In the period 2001–2004, movements in the source area were "very slow" to "slow" (following Cruden and Varnes 1996), ranging from 50 to 1,000 mm/year, with acceleration phases taking place mainly in autumn and late spring, after prolonged rainfall and/or snowmelt events. Hence, surges can be expected in the scenarios of extreme meteorological events and/or of excess pore pressure build-up due to activation of local shallow earthflows. This would imply a large amount of material to reach the track zone, with eventual total reactivation of the Corvara landslide and subsequent large damage. For this reasons, displacement rates in source area S3 have been monitored by RTK D-GPS during 15 monitoring campaigns carried out four to five times a year in the period from 2001 to 2004. Two master stations were set in stable areas outside the landslide. The displacement history of benchmarks 23–30 is plotted in Fig. 2, showing the norms of 3D displacement vectors for each measurement date and their directions. The gap periods of 10 months in the records are partly due to the existence of a thick snow cover in winter and spring seasons, during which measurements were not possible but significant displacements occurred. The data exhibit approximately linear trends. Rates of around 0.1 m/year were measured at benchmarks 24, 26 and 27, lying on the main landslide body of source area S3. Significantly higher displacement rates of around 0.2 m/year were observed in areas where, in addition to the movement of the main landslide body, the slope is also affected by shallow landslides (GPS benchmarks 23, 25 and 28). The GPS benchmarks 29 and 30, located in a relatively stable area below the crest of the slope and above the active part of source area S3, did not show significant displacements (Fig. 2).

Geological model of source area S3

A geological and geotechnical model of the whole Corvara landslide was made available by Panizza et al. (2006), including surface topography, stratigraphic profile, depth of sliding zones and dimensions of landslide bodies characterised by different displacement rates.

Surface topography was obtained by profiling a DEM produced in 2005 by the autonomous province of Bolzano using airborne LiDAR. Its nominal elevation accuracy is in the order of 1 m. A large number of geotechnical laboratory tests were carried out on samples of the landslide body in order to characterise the materials (grain size distribution, Atterberg limits, etc. on 25 soil samples, see Panizza et al. 2006) and assess shear strength (direct shear tests on 5 samples, see Panizza et al. 2006). Stiffness under different stress loads, consolidation behaviour and oedometric creep behaviour was analysed with oedometer tests, also with prolonged creep phases, isotropic compression and deviatoric creep tests (Schädler 2008). The landslide body is made up of a normally consolidated soil matrix of silty clays and clayey silts, which encloses coarser components, such as a variety of angular gravel-size particles, up to rock blocks. These consist of volcanoclastic and calcareous sandstones, marly limestones or dolostones. The mechanical behaviour of the shear zones is assumed to be mainly controlled by the properties of the clay-rich soil matrix (Table 1).

Underground boundaries, including the depth of sliding surfaces, have been obtained by interpreting field evidence, borehole stratigraphy, geoelectric and seismic refraction data, and inclinometer measurements. In source area S3, according to inclinometer C4 (Fig. 2), the landslide body is prevalently moving along a basal shear zone 40 m deep (Fig. 3). From inclinometer and TDR cables measurements, it can be inferred that the thickness of the main shear zones is in the order of 1 to 2 m (Corsini et al. 2005). In the lower part of source area S3, field evidence suggests that the landslide body thins out to a few metres due to the presence of a buried bedrock ridge. In the geological model, the basal surface of rupture of source area S3 is slightly dipping upslope in the foot area and outcropping upslope the track zone. In some sectors, a hummocky morphology and the presence of lateral ridges indicate that shallow earthflows are locally active over secondary shear zones, 3 to 10 m deep.

Below the main shear zone, old landslide material, colluvium and bedrock were found in borehole core of inclinometer C4. Since these materials gave very similar responses during the geophysical soundings (Panizza et al. 2006) and inclinometer C4 showed no movements below 40-m depth, when assigning properties to the different parts of the geological model, these materials were treated as one single unit (Fig. 3). Concerning hydrogeological conditions, two open pipe piezometers (in boreholes Cpz2 and C7) and one unsealed and uncemented inclinometer case operating as open pipe piezometer (C4) lie in source area S3 (Fig. 2, Table 2).

Measurement series recorded by electric transducers equipped with data loggers (acquisition time set to 30 min) indicated a groundwater depth varying from 0 to 8 m in the period 2001–2004 and revealed the existence of two different types of overlapping groundwater regimes. The first is connected to streams, ponds and marshes and therefore shows relatively small variations (C4 in Fig. 4); the second is linked to the infiltration of rainfall and consequently undergoes much larger seasonal fluctuations (Cpz2 in Fig. 4). In order to model the hydrogeological conditions for the entire 2D slope model, a single continuous aquifer marked by one average groundwater depth of 1 m was initially idealised. The geological and hydrogeological model of the slope is shown in Fig. 5.

Inverse parameter identification technique

Instead of varying the model parameters in a conventional, manual trial-and-error procedure, an inverse parameter identification approach using the back analysis method (Cividini et al. 1981) was applied to calibrate the numerical model of the slope and to back-calculate a subset of material parameters for which the available field measurements indicate a high sensitivity. The identification approach consists of a procedure performed in several substeps during which parameters are iteratively changed to achieve better fit between the model results and the field measurements. Goodness of fit is measured by the objective function $f(x)$, which has to be defined individually for each specific back-calculation task. The objective function used here is the mean-square deviation between monitoring data and simulation results. In order to confine the best fit searching procedure to reasonable solutions in physical and engineering terms, a bounded parameter search space Ω is defined.

Q3

Table 1 Average geotechnical parameters of the landslide material from source area

Parameter	Value
Unit weight γ	15–22 kN/m^3
Sand fraction	15 %
Silt fraction	50 %
Clay fraction	35 %
Lime content	39.7–55.5 %
Plasticity index	10–30 %
Natural water content	20–45 %
Plasticity Chart	MH-OH, ML-OL
Undrained cohesion c_u	30–100 kN/m^2
Effective peak friction angle φ'	20–30°
Effective peak cohesion c'	10–35 kN/m^2
Residual friction angle ϕ_r	15–20°
Modified compression index λ*	0.050–0.064
Modified swelling index κ*	0.020–0.035
Modified creep index μ*	8.09×10^{-4}–1.46×10^{-3}
Permeability k	2.10×10^{-10} m/s
Oedometer modulus E	5–53 MN/m^2
Shear modulus G	5,560 kN/m^2
Poisson's ratio v	0.35

From Corsini et al. (2005), Panizza et al. (2006), and Schädler (2008)

In this work, the solution of the optimisation problem (i.e., minimisation of the objective function) is based on a strategy called Shuffled Complex Evolutionary algorithm (SCE) proposed by Duan et al. (1992, 1993, 1994). The SCE belongs to a group of algorithms that combine methods and strategies of different optimisation algorithms in order to overcome weak points, restrictions and disadvantages of the individual methods when used alone. Prior to the application of an optimisation scheme to a back-calculation problem, it is highly recommended to gain more information on the initially unknown objective function topology. For this purpose, a number of forward calculations are performed using randomly chosen parameter sets within physically reasonable ranges, and the objective function value is calculated for each parameter set. To visualise this kind of multi-dimensional data, a scatter-plot matrix as shown in Fig. 6a is often used. In this type of scatter-plot matrix, each row and column correspond to one parameter being varied, where each subplot can be interpreted as projection of the multi-dimensional objective function topology (Manly 1944). To avoid appending an additional row to the matrix showing the objective function value on its vertical axis, these plots are moved to the diagonal elements of the plot matrix. For each forward calculation of the randomly chosen parameter sets, one data point can be plotted in each of the subplots of a scatter-plot matrix. To allow for an assessment of the distribution of a certain objective function value range, a filtered subset of the randomly chosen parameter sets is usually plotted. If only the best items are plotted, the resulting point clouds give an impression of the optimal objective function value range.

For example, a simple analytical function is used for generating the scatter-plot matrix of Fig. 6, where only parameter sets are shown leading to $f(x)\leq 0.5$ (10,000 parameter sets had been calculated within $-1\leq x_{1,2,3}\leq +1$ of which 281 sets satisfy $f(x)\leq 0.5$). The three columns and rows of Fig. 6a correspond to the parameters x_1, x_2 and x_3 of the objective function. As visible from Fig. 6b, the optimal value range envelopes show a "correlation" between x_1 and x_3. Additionally, from the analytical function, it is to be

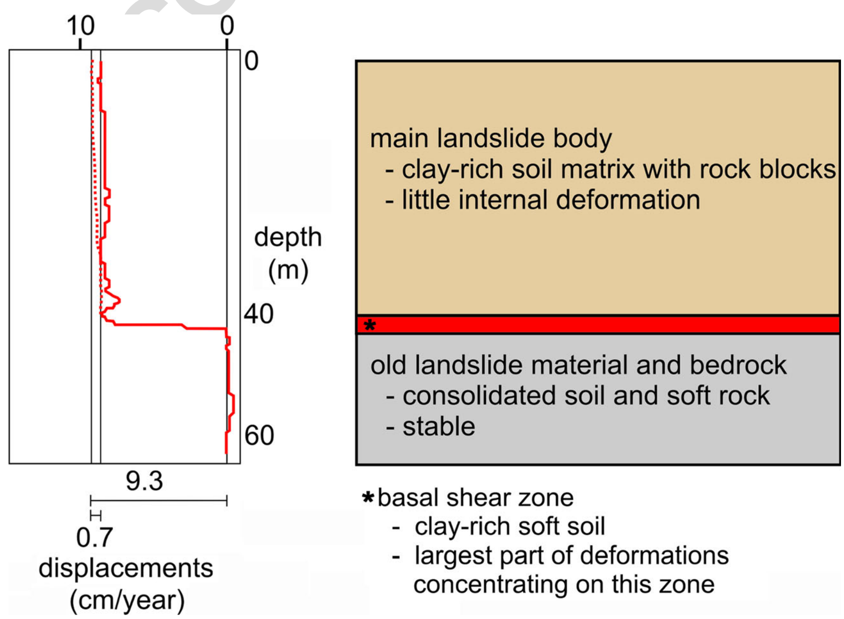

Fig. 3 Internal stratification of the geological model (inclinometer data from Corsini et al. 2005 and Panizza et al. 2006). *Solid red line* indicates inclinometric profile and layering observed along the entire length of the tube; *dotted red line* indicates inclinometric profile after the rupture of the tube at 40-m depth

Table 2 Groundwater monitoring devices

Label	Diameter (inch)	Depth (m)	Type
C4	2	60	Unsealed/uncemented inclinometer case operating as open pipe piezometer
Cpz2	2	45	Open pipe piezometer fissured only at 39–45-m depth
C7	4	88	Open pipe piezometer

expected that x_1 is the least and x_3 is the most sensitive parameter for $f(x)$. The following statements hold:

- The projected shapes of the isosurfaces for $f(x)=0.5$ of Fig. 6b correspond very well to the envelopes of the point clouds of the individual subplots of Fig. 6a.
- The correlation of x_1 and x_3 is nicely visible in the corresponding subplots and for the point cloud shown; a 2D linear correlation coefficient of −0.74 is calculated. As to be expected, for the other parameter combinations, no correlation is visible.
- The diagonal elements of the scatter-plot matrix provide insight to the local sensitivity of the objective function range shown for x_1, x_2 and x_3. First, only one lower tip of the point cloud envelope is visible, what indicates that only one optimum is existing within the investigated range. Second, as more sensitive a parameter is, as more "pointy" the lower tip of the point cloud envelope should be. As expected, x_1 is the least and x_3 is the most sensitive parameter. In general, if an inverse problem is well posed, each of the diagonal plots should present one firm extreme value. Otherwise, the respective parameter may not be identified reliably.
- The diagonal elements of the scatter-plot matrix indicate that the global optimum is somewhere near $x_1=0$, $x_2=0$ and $x_3=0$.

This kind of statistical analysis of the results of forward calculations can be used to determine those parameters which are indifferent to the system response or dependent on each other. These parameters can be removed prior to back-calculation. Furthermore, the remaining parameters can be classified according to their influence (Schwarz 2001).

Forward calculations

Hydrogeological model

Steady state and transient groundwater flow calculations were carried out applying the FE code SEEP/W (Krahn 2004). Zero flow

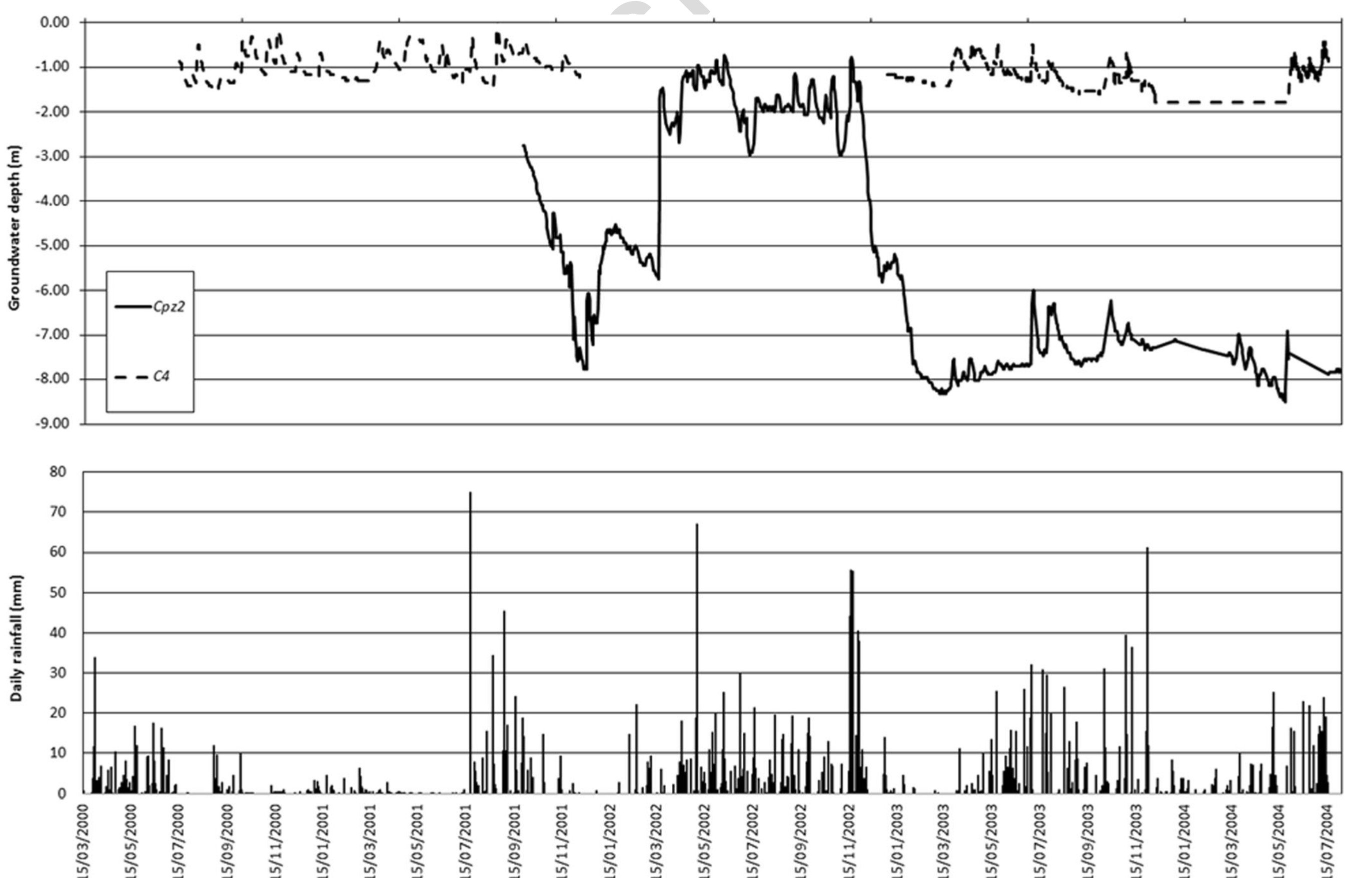

Fig. 4 Piezometric data and rainfall during 2001–2004 monitoring period

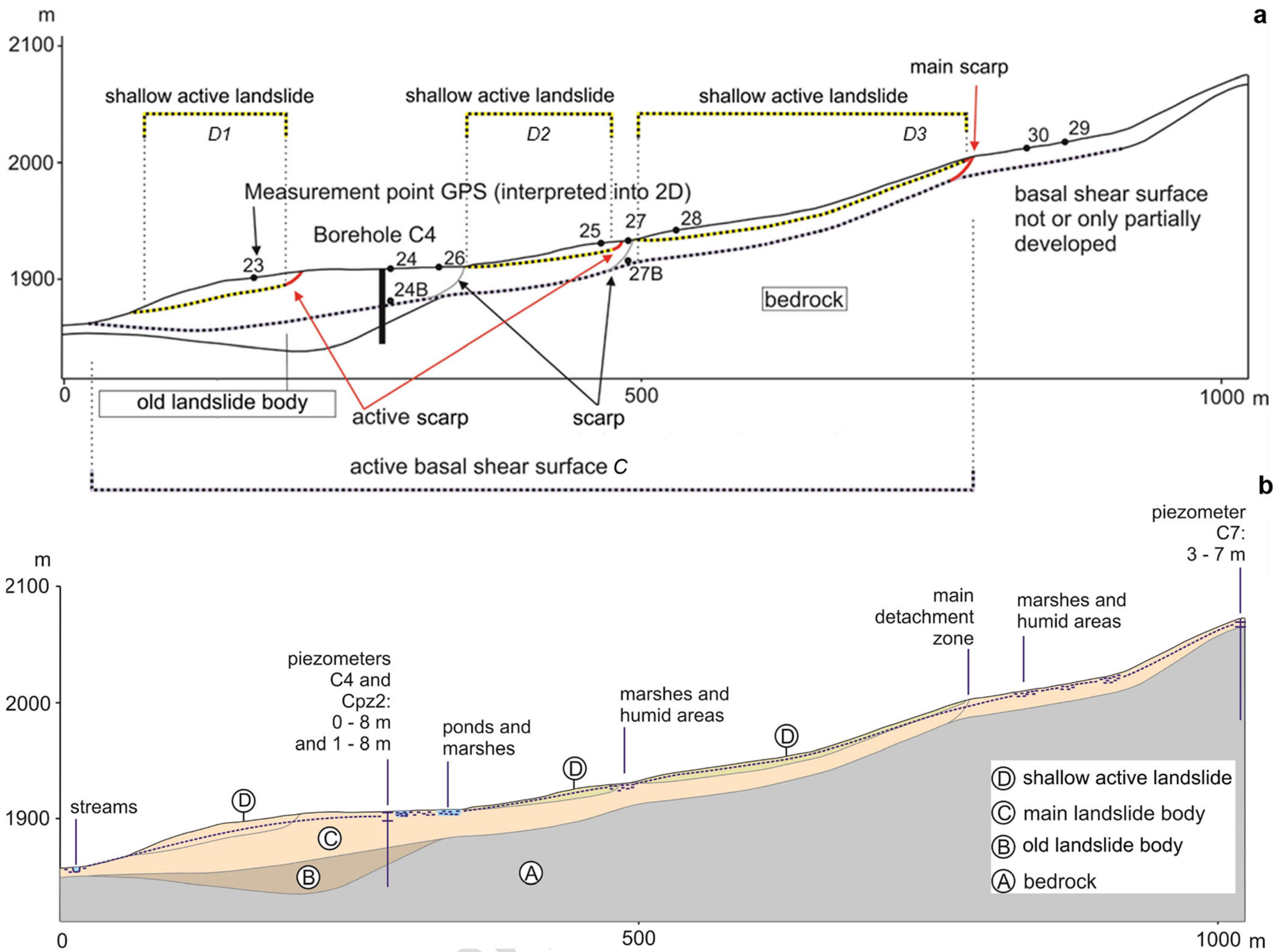

Fig. 5 **a** 2D geological model of source area S3. See Fig. 2 for location. Point 24B is based on inclinometric measurements. **b** Simplified hydrogeological model assuming an average water table to be implemented in the seepage model (piezometer data from Panizza et al. 2006)

was allowed through the basal boundary of the geological model, and fixed groundwater heads were prescribed at its lateral boundaries based on monitoring data. Water levels were then generated by means of a 2D slope infiltration and seepage model. Input flow rate was calculated monthly according to the Thornthwaite (1948) formula, using rainfall, snowmelt and temperature data recorded at the on-site meteorological station (observation period 2001–2004, Table 3).

The calculated effective recharge was simulated using a transient flux boundary condition applied at each node on the slope surface profile (q in m/s, see Krahn 2004). At every node, the potential seepage review boundary condition was adopted in order to avoid ponding. A null-flux condition was imposed at the base of the model and at the upslope model boundary because the crest of the slope was assumed to represent the main water divide. The model parameters (saturated and unsaturated hydraulic conductivities, volumetric water content functions and conductivity functions, here represented by a straight line) were estimated from grain-size distributions, Atterberg limits, water content at saturation and coefficient of volume compressibility of the landslide materials. Recommendations within Krahn (2004) and data proposed by other authors (e.g. Caris and van Asch 1991; Bonomi and Cavallin 1999; Malet et al. 2005; Tacher et al. 2005; Francois et al. 2007) were also considered. In order to further simplify the hydrogeological model, isotropic hydraulic permeability was assumed for all materials, except for shallow landslide bodies in which the vertical permeability was assumed to be three times higher than the horizontal one (Table 4).

The infiltration and seepage model was calibrated by a trial-and-error procedure against the monitoring data of piezometer Cpz2, in which groundwater level is largely controlled by infiltration (Fig. 4). Calibration was continued until an acceptable fit between calculated and measured level was obtained for the recharge as well as for the discharge curve (Fig. 7). Conservative hydrostatic pore pressure distributions were then used in the deformation model.

Finite element hydraulic-mechanical model

The kinematics of the slope during the observation period (2001–2004) were simulated using the FE method. All calculations were carried out using the Plaxis~~code~~ version 8.2 (2003), taking into account the effect of large deformations by means of an updated Lagrangian formulation (updated mesh analysis). Calculations

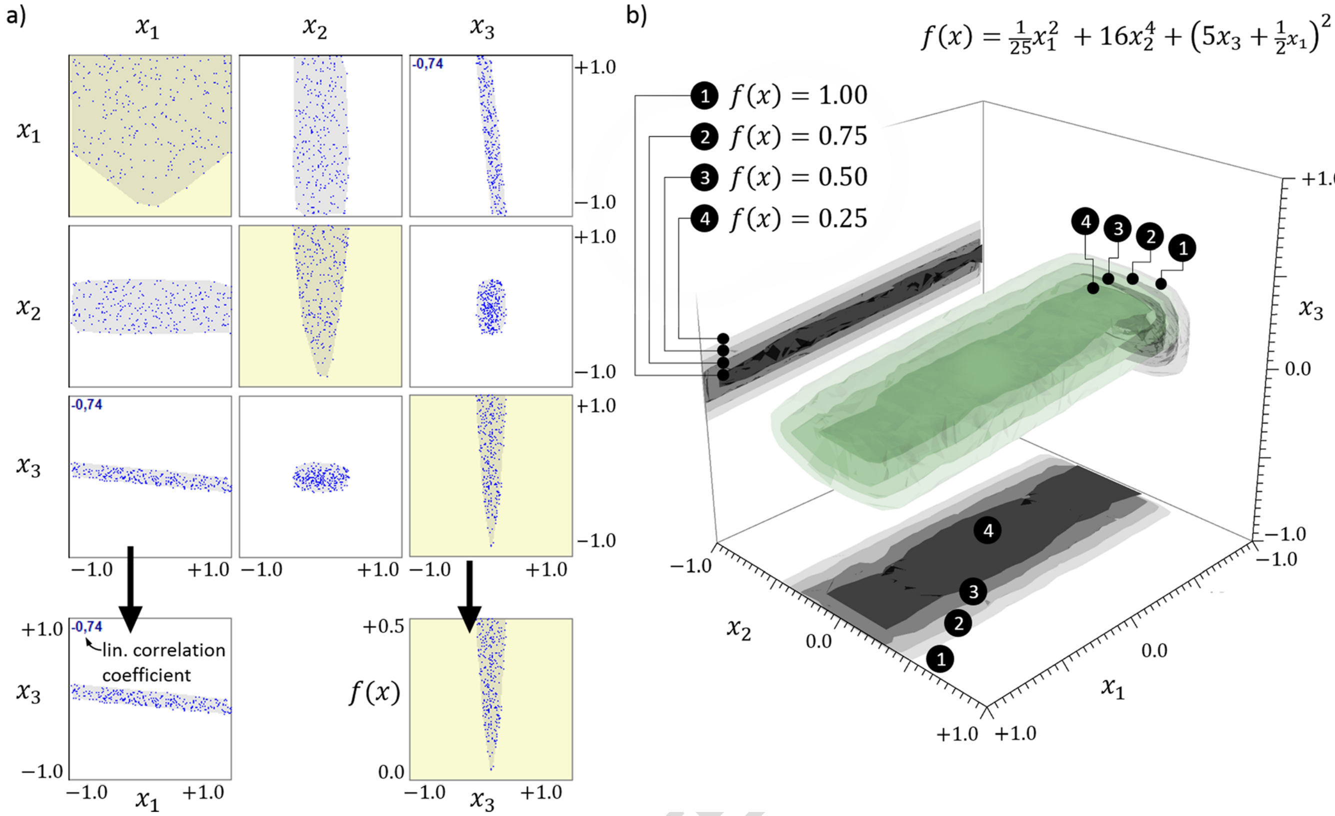

Fig. 6 Scheme of the scatter-plot matrix. **a** Multi-dimensional data plotted in a scatter-plot matrix. **b** Example of the objective function calculation for a simple analytical function

were performed as consolidation analyses, i.e. modelling the stress–strain field and taking into account the time-dependent development of pore pressures. A plane-strain geometrical configuration with the real dimensions of the slope was used. The model was discretised using 2790 triangular 15-node elements. Horizontal deformation fixities were assigned to the lateral boundaries and total deformation fixities to the basal boundary.

Based on lab tests (Table 1) and on the results of calibration of the constitutive model (Schädler 2008), the soil along the shear zones can be regarded as a plastic material, which is characterised

t3.1 **Table 3** Average climatic data for the observation period. The calculated effective recharge was used as input in the infiltration and seepage model

Month	Mean monthly air temperature (°C)	Mean monthly rainfall (mm)	Mean monthly snowmelt (mm)	Mean monthly evapotranspiration (mm)	Mean monthly effective recharge (mm)	t3.2
Jan	−4.7	29.0	0.0	0.8	28.1	t3.3
Feb	−3.1	29.1	10.3	1.1	38.4	t3.4
Mar	0.5	46.8	22.9	7.4	62.3	t3.5
Apr	2.7	54.1	6.1	30.1	30.1	t3.6
May	8.3	92.5	0.0	92.5	0.0	t3.7
June	12.4	82.4	0.0	82.4	0.0	t3.8
July	13.4	97.9	0.0	97.9	0.0	t3.9
Aug	14.1	75.9	0.0	75.9	0.0	t3.10
Sept	9.0	80.5	0.0	80.5	0.0	t3.11
Oct	5.4	69.8	0.0	50.6	19.1	t3.12
Nov	0.8	149.6	11.0	4.9	155.8	t3.13
Dec	−2.5	39.1	20.3	1.1	58.3	t3.14
Total		846.6	70.7	524.5	392.2	

Table 4 Saturated hydraulic conductivity values used in the trial-and-error procedure for the calibration of the steady-state groundwater flow calculation

Layer		Fixed values and constraints (m/day)	Calibrated values (m/day)	Adopted values (m/s)
D	Active shallow landslide bodies	D2 > D1; <0.09	0.03	3.47E-07
		D1 ≥ C	0.01	1.16E-07
C	Main landslide body	0.009		1.04E-07
B	Old landslide body	A < B < C	0.004	4.63E-08
A	Bedrock	0.0009		1.04E-08

D1 horizontal, *D2* vertical

by a pronounced time-dependent behaviour (Picarelli et al. 2000; Augustesen et al. 2004). Therefore, the Soft Soil Creep model was used as a constitutive model for these zones (Vermeer and Neher 1999). A set of three parameters (effective cohesion c, effective friction angle φ and dilatancy angle ψ) is required to model failure according to the Mohr-Coulomb criterion. Two further parameters are used to model the amount of plastic and elastic strains and their stress dependency. The modified compression index (λ^*) represents the slope of the normal consolidation line. The modified swelling index (κ^*) is related to the unloading or swelling line. The modified creep index (μ^*) measures the development of volumetric creep deformations with the logarithm of time.

Due to the age of the landslide activity in source area S3 and the continuous nature of the sliding processes, it was assumed that in the long term, the shear zones have undergone relative displacements in the range of at least tens of metres. Therefore, the material of the shear zones is assumed to have reached the residual strength. As the subsoil away from the shear zones shows little internal deformations (Fig. 3), the material behaviour was modelled as linear-elastic to account for the gravitational loads that these materials exert onto the shear-zone layers.

The initial stress state at the beginning of the modelled time span, i.e. in the year 2001, is mainly a consequence of the long-term history of the slope. Therefore, the initial stress state in the model was generated by simulating a simplified loading history, based on the knowledge about the slope evolution. Modelling ~~of the different phases~~ was performed in six phases: gravity loading, unloading by weathering and erosion, loading by glaciers, formation of weak zones, unloading after glaciation and creeping. It was assumed that already prior to the last glaciation, the slope was characterised by a gently inclined profile. Therefore, in a first calculation phase, a stress field was created by gravity loading based on the actual topography and assuming a homogeneous linear elastic material, whose specific weight equals that attributed to the actual bedrock. During gravity loading, Poisson's ratio was adjusted to result in a ratio between horizontal and vertical stresses corresponding approximately to a K_o value of 0.8. Then, the value of Poisson's ratio was changed to the assumed current value (0.33), which was then used in further calculation phases. In a second calculation phase, the slope model was unloaded by lowering the specific weight of all layers, except for the bedrock, to present-day values. In a third phase, a distributed load of 1,000 kN/m^2 was applied perpendicularly to the ground surface to simulate loading by Pleistocene glaciers. In a fourth phase, weak layers were inserted into the model as a result of deep weathering during the glaciation and deglaciation phases. In a fifth phase, the slope was unloaded very fast to its actual state immediately after the shear-zone layers had been inserted. In a sixth phase, the shear-zone materials were left creeping under the assumed average water pressures until approximately constant displacement rates were observed with respect to the time-scale of the simulated monitoring period. The duration of this phase (10,000 days, approx. 27 years) had to be defined arbitrarily to comply with this criterion. The stress state reached at the end of this last phase of the loading history was taken as initial stress state for the simulation of deformations in the monitoring period.

A first-trial forward calculation, using parameter values directly from the laboratory tests, was carried out (Table 5). The calculated total displacements at the end of the 3 years of the monitoring period appeared to be underestimated by the model, with total displacements in the order of 7 cm with respect to 30–70 cm measured in the field. Anyhow, in the most active region, the shape of the displacement profile and the direction of displacement vectors were in qualitative agreement with the measurements.

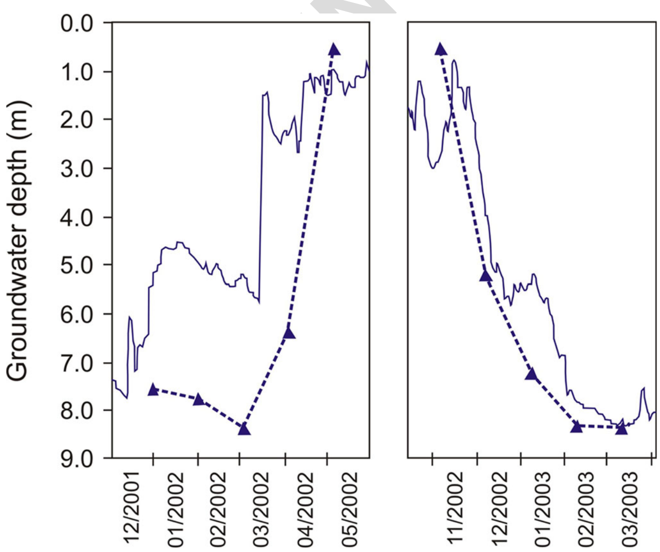

Fig. 7 Observed and calculated groundwater depths in borehole Cpz2 from December 2001 to March 2003 during recharge and discharge phases

Inverse analysis

Statistical analysis

The results of the first-trial calculation suggest that the material parameters are not the same for all shear zones (i.e. basal shear zone C and shear zones of shallow active landslides D1, D2 and D3, t5.1 **Table 5** Experimental parameter values used for all the shear zones in the first-trial forward calculation. Shear strength parameters from Panizza et al. (2006) and stiffness parameters and creep parameters by oedometer tests in Schädler (2008), as shown in Table 2

	Material parameter	Value
t5.2	Material parameter	Value
Q2/ t5.3	λ^*	0.057
t5.4	κ^*	0.028
t5.5	μ^*	1.2×10^{-3}
t5.6	Φ	20°
t5.7	c	27 kN/m^2
	ψ	0°

see Fig. 5). Hence, in the statistical analysis of the model behaviour, some of the parameters were correlated, while others were chosen to be identified independently, trying to minimise the number of variable parameters, but not to oversimplify the model.

The displacement rates depend on shear strength and creep behaviour of the shear zones, which is in turn controlled mainly by the modified creep index μ^* and is also related to their stress-dependent compressibility and vice versa. The latter is described by the modified compression index λ^*. This means that λ^* and μ^* depend on each other or the ratio of them is about constant (Mesri and Godlewski 1977; Mesri and Castro 1987). Both parameters are unknown along the shear zones of landslide source area S3. They were identified by varying them within large search intervals

Table 6 Search intervals and fixed parameters used for the statistical analysis and the optimisation procedure (in *grey*, the eight parameters to be identified) t6.1

material	parameter	unit	fixed value	vary between				constraint
				min.	max.	ln (min.)	ln (max.)	
C basal shear-zone	λ* (C)	none		0.04	1	-3.22	0	
	κ* (C)	none	0.02					
	μ* (C)	none		0.001	0.5	-6.91	-0.69	μ* (C) < 0.5 λ* (C)
	φ (C)	°		15	25			
	c (C)	kN/m²	0.3					
D1 secondary shear-zone of front block	λ* (D1)	none	λ* (D1) = λ* (C)					
	κ* (D1)	none	0.02					
	μ* (D1)	none	μ* (D1) = μ* (D2)					
	φ (D1)	°		15	25			
	c (D1)	kN/m²	0.3					
D2 secondary shear-zones of active shallow landslides	λ* (D2)	none		0.04	1	-3.22	0	λ* (D2) > λ* (C)
	κ* (D2)	none	0.02					
	μ* (D2)	none		0.001	0.5	-6.91	-0.69	μ* (D2) < 0.5 μ* (C)
	φ (D2)	°		15	25			
	c (D2)	kN/m²	0.3					
D3 secondary shear-zone (uppermost part)	λ* (D3)	none	λ* (D3) = λ* (D2)					
	κ* (D3)	none	0.02					
	μ* (D3)	none	μ* (D3) = μ* (D2)					
	φ (D3)	°	φ (D3) = φ (D2)					
	c (D3)	kN/m²		5	50			

In spite of linking a number of parameters, still, eight parameters remain to be identified, namely λ^* (C), μ^* (C), φ (C), φ (D1), λ^* (D2), μ^* (D2), φ (D2) and c (D3). A statistical analysis, based on 7,670 calls of the forward calculation, was carried out on these eight parameters, varying them within the intervals specified in Table 6. The corresponding scatter-plot matrix is presented in Fig. 8

(Table 6). As a result of the long-term displacements (up to 75 cm in 2001–2004 monitoring period), residual strength conditions were assumed. Accordingly, an arbitrary value of 0.3 kN/m² has been used for residual cohesion in order to avoid numerical instability in the calculations. Due to the situation that in shear-zone domain D3, the activity rate is lower (cumulative displacements from 5 to 30 cm in 2001–2004 monitoring period) ~~and~~ it was assumed that the corresponding shear surface is not fully developed and strength is not fully softened. Therefore, a search interval for cohesion also was adopted here (Table 6). Representative values of the friction angle ϕ are assumed to be controlled also by the presence of coarser components, such as rock blocks. Consequently, the friction angles of the shear zones were selected to be identified, varying them between 15° and 25°, i.e. the estimated residual friction angle of the soil matrix and the friction angle of bedrock in heavily weathered condition (Panizza et al. 2006). The modified swelling index of κ^* was fixed based on laboratory data: Values obtained in five oedometer tests on different samples from the soil matrix of the landslide material (fraction <2 mm) ranged between 0.01 and 0.05, with an average value of 0.026. Due to the influence of less deformable coarser components, representative values of κ^* for the shear zones were assumed to be lower, i.e. stiffness is higher than that of the fine-grained fraction. Therefore, the value of 0.02 was used. To avoid physically and numerically unfavourable parameter combinations and to minimise the number of unsuccessful attempts, two parameter constraints were prescribed in all parameter sets, based on literature and lab data: The highest μ^* value be smaller than half of the lowest λ^* value. A

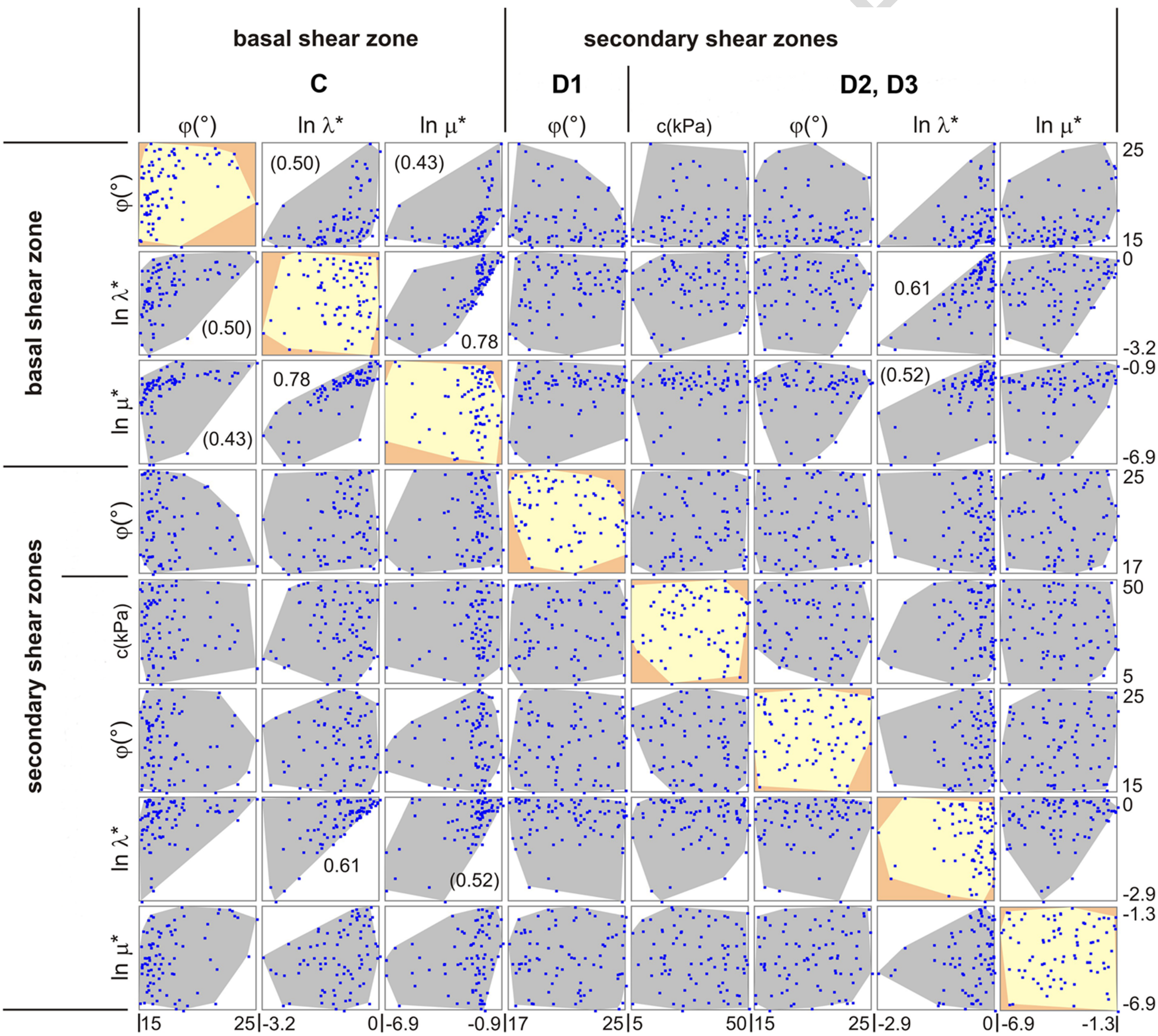

Fig. 8 Scatter-plot matrix for the slope model. Basal shear zone C and Secondary shear zones D1, D2 and D3 (see Fig. 5 and Table 6). The numbers are 2D linear correlation coefficients as described in Section 3 and Fig. 6. In case the coefficient falls below 0.6, the numbers are in *brackets*. In case the coefficient is below 0.3 no number is shown

summary of all above-described parameter links and parameter constraints is given in Table 6.

To indicate the expected shape and location of the optimal value range, this matrix shows only the parameter combinations related to the 83 lowest objective function values (marked by blue points in the matrix). None of the plots of the scatter-plot matrix have a clear-cut shape; therefore, the problem must be considered as underdetermined and it is advisable not to increase the number of varying parameters. However, the objective function plots give some pieces of information as to the most probable ranges of the best parameter values. For the friction angle φ of the basal shear zone C, the best parameter sets are all located in the lower part of the search interval, i.e. between 15° and 19°, whereas for μ^* of this zone, they accumulate in the upper part of the interval. Less clearly, this can be noticed also for the values of λ^*, because μ^* and λ^* appear to be correlated (linear correlation coefficient of 0.78), as previously expected. None of the 83 best parameter combinations have a value of μ^* in the uppermost part of the search interval, i.e. between logarithmised μ^* values of −0.9 and −0.69. The information obtained for the parameters of the secondary shear zones D1, D2 and D3 is less clear. As in none of the displayed best parameter sets φ of the front slide (D1) is below 17° and furthermore in 15 of the 18 best sets, φ values are between 18° and 23°, and the statistical analysis indicates that an optimum value of this parameter can be identified in the medium range of the search interval. Relatively good objective function values can be obtained independent of the cohesion value assigned to shear-zone domain D3, except for values from the lowermost part of the interval. In contrast, relatively good fits are observed for a wide range of friction angles of D3 but not for values from the uppermost part of the search interval. In the case of λ^* for shallow landslides, the accumulation of plotted points on the right side of the interval as well as the weak correlation between $\lambda^*(C)$ and $\lambda^*(D2, D3)$ are direct consequences of the parameter constraint demanding for $\lambda^*(D2, D3) > \lambda^*(C)$. The objective function projection for the parameter μ^* of these layers shows good model fits independent of the parameter value, except for the uppermost part of the search interval (between logarithmised μ^* values of −1.3 and −0.69) where none of the 83 best parameter sets are plotted. From the scatter-plot matrix in Fig. 8, it is not clear whether the search interval for λ^* of the shear zones of the shallow landslides (D2 and D3) is sufficient since the data points with low deviation values accumulate near the upper boundary. As for higher values of λ^* (e.g. between 1 and 2, logarithmised values between 0 and 0.69), the percentage of failed forward calculations increased considerably and it was decided not to enlarge the interval.

Identification of shear-zone parameters with the SCE algorithm

After the statistical analysis, the search intervals presented in Table 6 were used also for the optimisation procedure applying the SCE algorithm, as described in the "Inverse parameter identification technique" section. After 1,100 calls of the forward calculation, the SCE algorithm was not able to further reduce the objective function value. The lowest value reached 9.2×10^{-4}. The parameter sets identified by the algorithm using the complete reference dataset are shown in Table 7.

Table 7 Relative errors between simulated horizontal displacements and GPS measurements at points 23–28 [(measured − calculated) / measured] in the two steps of the calibration procedure (1: first step optimisation; 2: second step optimisation)

GPS point	Step	GPS Survey										
		Sep 01	Jun 02	Aug 02	Sep 02	Oct 02	Jun 03	Aug 03	Sep 03	Jun 04	Aug 04	Oct 04
23	1	0	−0.11	−0.12	−0.13	−0.15	−0.01	−0.01	−0.02	0.11	0.15	0.11
	2	0	−0.18	−0.18	−0.19	−0.20	−0.11	−0.11	−0.11	0.02	0.07	0.01
24	1	0	−0.72	−0.28	−0.32	−0.31	−0.07	−0.21	−0.18	0.02	0.04	0.03
	2	0	−0.78	−0.37	−0.40	−0.39	−0.10	−0.27	−0.24	−0.01	0.00	0.00
25	1	0	−0.38	−0.34	−0.35	−0.45	−0.04	−0.09	−0.08	0.07	0.05	0.04
	2	0	−0.52	−0.45	−0.45	−0.57	−0.13	−0.18	−0.17	0.00	−0.03	−0.04
26	1	0	−0.50	−0.43	−0.27	−0.30	−0.05	−0.17	−0.09	0.10	0.08	0.10
	2	0	−0.56	−0.54	−0.36	−0.40	−0.09	−0.24	−0.16	0.06	0.03	0.06
27	1	0	−2.54	−0.80	−0.79	−0.88	−0.27	−0.30	−0.39	−0.13	−0.14	−0.10
	2	0	−2.97	−0.98	−0.95	−1.04	−0.40	−0.41	−0.50	−0.22	−0.23	−0.20
28	1	0	−1.11	−0.74	−0.84	−0.82	−0.04	−0.03	−0.06	0.11	0.22	0.21
	2	0	−1.44	−0.97	−1.08	−1.06	−0.19	−0.17	−0.20	−0.02	0.10	0.09

In the second step optimisation, a narrowed dataset was used (GPS benchmarks 23, 25 and 28)

In Fig. 9, the results of a calculation using the best parameter set of the first step of the optimisation procedure can be compared to the measured horizontal displacements of GPS points 23 to 28. Considering the simplifications made in the model, it can be stated that displacements are reproduced quite well for most points, but underestimation occurs at GPS points 23 and 28. As these points lie above secondary shear zones, in a second step of the optimisation procedure, the parameters of the basal shear zone were fixed at the identified best values. In this phase, a narrowed dataset was used, containing only horizontal displacements of the three measurement points located above secondary shear zones (points 23, 25 and 28). A total of six parameters were varied in the second step of the optimisation procedure. For the search, the configuration of parameter links, parameter constraints and search intervals was in fact modified in some details: The optimisation algorithm was allowed to vary the friction angle of D3 shear-zone domain independently of that of D2. When fixing the parameters of the basal shear zone, the parameter constraint demanding for $\lambda^*(C)<\lambda^*(D2, D3)$ was removed because it was preferred not to restrict the search based on a value of an identified parameter set. After 2,092 calls, the optimisation was stopped because no

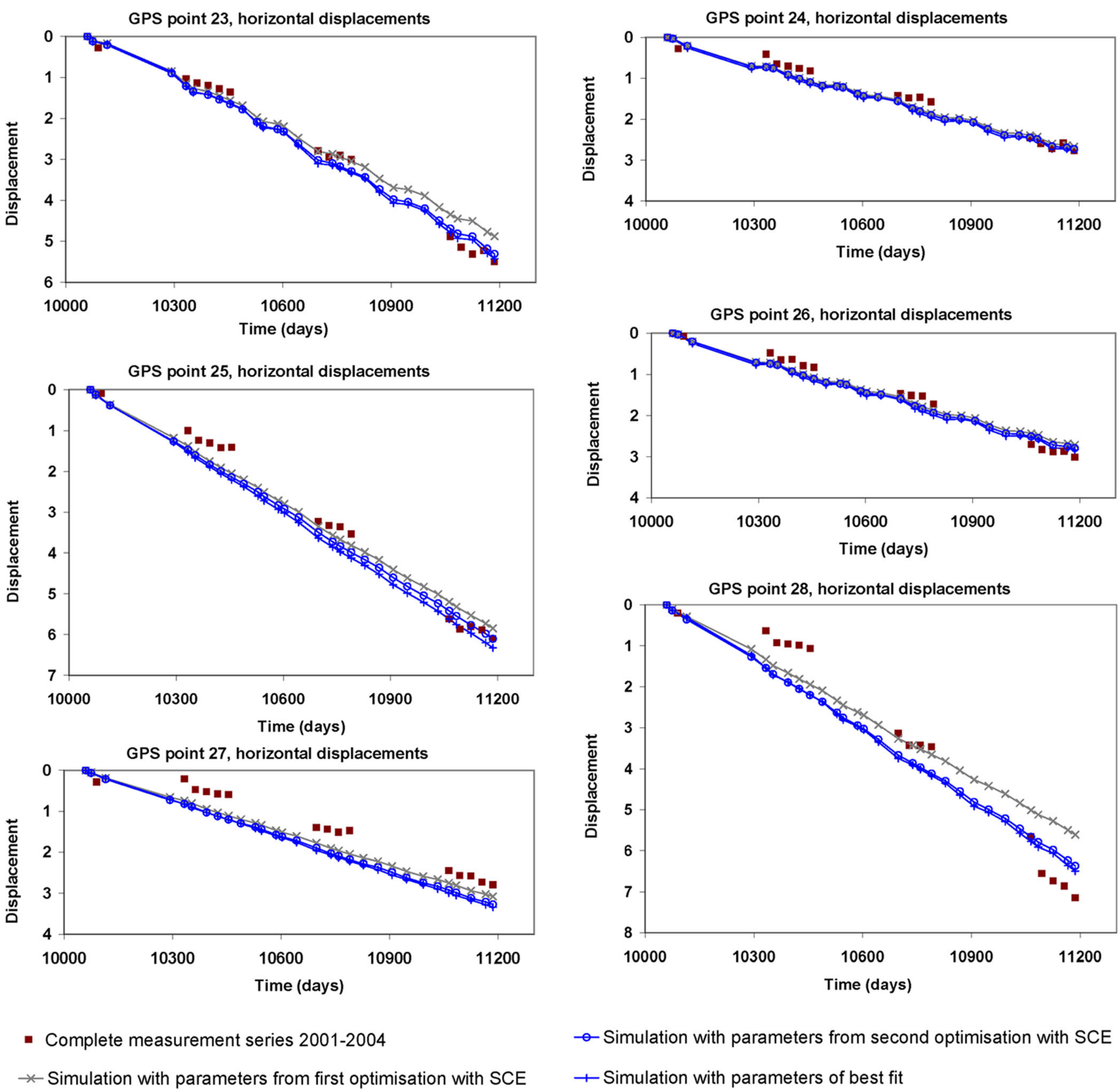

Fig. 9 Time series of calculated displacements and measured data for GPS points 23–28 (displacements in dm)

Table 8 Summary of parameter values identified with SCE algorithm for the slope model

Parameter (unit)	λ^*		μ^*		Φ (°)				c (kN/m^2)
Zones	C, D1	D2, D3	C	D1, D2, D3	C	D1	D2	D3	D3
Complete dataset	0.62	0.96	0.17	0.31	18.1	21.6	16.2	16.2	48.3
Narrowed dataset	Fixed	0.63	Fixed	0.24	Fixed	19.5	16.4	23.8	16.9

significant reduction of the objective function value was observed. It can be noticed that the underestimation of displacements at points 23 and 28 is reduced after the second step optimisation. The relative errors between simulated and measured values are shown in Table 7, with maximum relative errors in the order of 20 % at the end of the simulated monitoring period. The identified best parameter set is given in Table 8.

In Fig. 9, the second-step optimisation results are compared to the measured time series of the horizontal displacements at GPS benchmarks 23–28 (2001–2004 displacements are shown at the same timescale for all points). For GPS benchmarks 23, 24, 25 and 26, the whole curve of the time series is nearly matching the reference data points, except for small differences, which are always below 5 cm. These benchmarks are located in the slope area where most of the hydrogeological data have been collected; hence, the simplified hydrological assumptions hold true. Conversely, the calculated displacement patterns are not curved enough, or too linear, at GPS points 25, 27 and 28. There, the displacements are smaller in summer and larger during autumn and after snowmelt infiltration. Due to the simplified hydrogeological assumptions, this seasonal phenomenon is not reproduced properly by the model. In Fig. 10, the displacement vectors calculated for the 3 years of the monitoring period (2001–2004) after the second step of optimisation are compared with those measured in the field by means of GPS. Reproduction of the horizontal displacements at the end of the monitoring period is good. Except for GPS points 26 and 28, vertical displacements are clearly overestimated, even if the low precision of the vertical displacement measurements has to be taken into account. However, the direction of the simulated displacements is subparallel to the slope, as observed in the source area of the Corvara earthflow. Qualitatively, the modelled displacement profile at point 24 is in accordance with that measured by the nearby inclinometer C4.

Conclusions

The case study of the Corvara earthflow is promising, as a large amount of relevant high-quality data, obtained at several locations, mainly with continuous or semi-continuous acquisition frequency, are available. In fact, geomorphological evidence and monitoring data at the local scale were exploited in support of the development, running, calibration and validation of an FE continuum model. In particular, the model calibrated via an inverse parameter identification technique was able to simulate the displacement occurred at several monitoring points in the source area S3 with average relative errors for horizontal displacements at the end of the simulated period lower than 7 %.

Applying the inverse analysis makes the calibration procedure much more objective and repeatable. Beyond that, these methods provide statistical information about sensitivity and interdependence of model parameters. In principle, the definition of the overall modelled problem improves with any additional value measured in the field, and calibration quality can be quantified via the objective function. Obviously, an increase of the temporal resolution of the displacement measurements and of the spatial resolution of the pore pressure measurements could improve the calculated displacements obtained in this study. The longer and the more comprehensive the time series of measurements are, the more parameters can be identified, which until now had to be fixed based on assumptions. Quantitative results—objective function values, correlations, etc.—obtained by the statistical analyses and during the optimisation allow for judging whether a refinement of the model

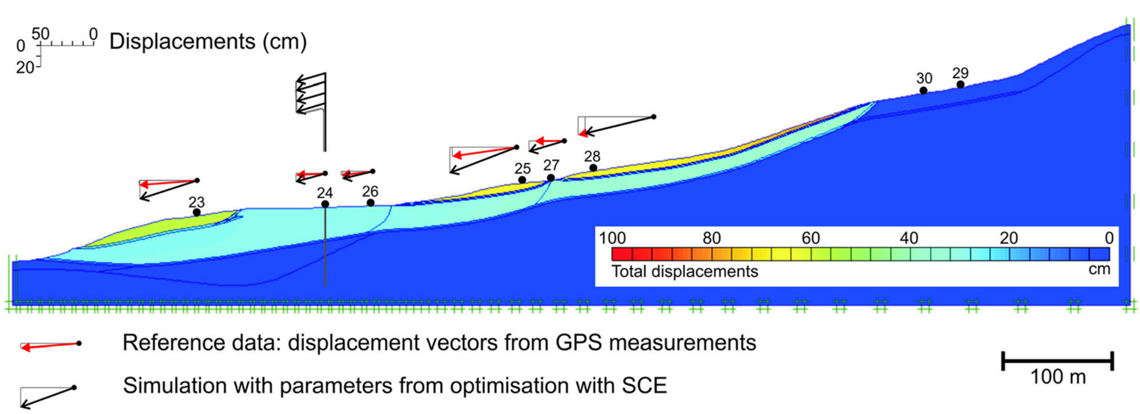

Fig. 10 Calibrated slope model. Comparison of simulated displacement vectors with GPS field measurements during 2001–2004 period

improves its quality or if an apparently more realistic model will lead to further uncertainty. This type of information can hardly be gained when model calibration is performed by means of a traditional trial-and-error procedure.

Acknowledgments

The German Academic Exchange Service (DAAD) and the Ateneo Italo-Tedesco are acknowledged for funding a VIGONI 2006–2007 exchange project. DAAD granted a short research period to L. Borgatti in 2013 which was useful to finalise the paper. Six anonymous reviewers and the editor are acknowledged for their constructive comments.

References

Angeli MG, Gasparetto P, Pasuto A, Silvano S, Menotti RM (1996a) Examples of mudslides on low-gradient clayey solpes. In: Senneset K (ed) Landslides, Proc. 7th Int. Symp. Landslides, Trondheim. Balkema, Rotterdam 1:141–145

Angeli MG, Gasparetto P, Menotti RM, Pasuto A, Silvano S (1996b) A visco-plastic model for slope analysis applied to a mudslide in Cortina d'Ampezzo, Italy. Q J Eng Geol 29:233–240

Angeli MG, Buma J, Gasparetto P, Pasuto A (1998) A combined hillslope hydrology/stability model for low-gradient clay slopes in the Italian Dolomites. Eng Geol 49:1–13

Augustesen A, Liingaard M, Lade PV (2004) Evaluation of time-dependent behaviour of soils. Int J Geomech 4(3):137–156

Bonomi T, Cavallin A (1999) Three-dimensional hydrological modelling application to the Alverà mudslide (Cortina d'Ampezzo, Italy). Geomorphology 30:189–199

Borgatti L, Soldati M (2010) Landslides as a geomorphological proxy for climate change: a record from the Dolomites (Northern Italy). Geomorphology 120:56–64

Borgatti L, Corsini A, Marcato G, Pasuto A, Silvano S, Zabuski L (2007a) Numerical analysis of countermeasure works influence on earth slide stabilisation: a case study in South Tyrol (Italy). In: Proceedings of the First North American Landslide Conference (ed) Landslides and Society: Integrated Science, Engineering Management and Mitigation. AEG, Vail (USA) 23:1007–1015

Borgatti L, Ravazzi C, Donegana M, Corsini A, Marchetti M, Soldati M (2007b) A lacustrine record of early Holocene watershed events and vegetation history, Corvara in Badia, Dolomites (Italy). J Quat Sci 22(2):173–189

Calvello M, Finno RJ (2004) Selecting parameters to optimize in model calibration by inverse analysis. Comput Geotech 31:411–425

Caris JPT, van Asch T (1991) Geophysical, geotechnical and hydrological investigations of a small landslide in the French Alps. Eng Geol 31(3–4):249–276

Cividini A, Jurina L, Gioda G (1981) Some aspects of characterization problems in Geomechanics. Int J Rock Mech Min Sci 18(6):487–503

Comegna L, Picarelli L, Urciuoli G (2007) The mechanics of mudslides as a cyclic undrained–drained process. Landslides 4(3):217–232

Corsini A (2000) L'influenza dei fenomeni franosi sull'evoluzione geomorfologica post-glaciale dell'Alta Val Badia e della Valparola (Dolomiti). Dissertation, Università di Bologna, Italy

Corsini A, Pasuto A, Soldati M (1999) Geomorphologicalinvestigation and management of the Corvara landslide (Dolomites, Italy). Trans Jpn Geomorphol Union 20:169–186

Corsini A, Marchetti M, Soldati M (2001) Holoceneslopedynamics in the area of Corvara in Badia (Dolomites, Italy). Geografia Fisica e Dinamica Quaternaria 24:127–139

Corsini A, Pasuto A, Soldati M, Zannoni A (2005) Field monitoring of the Corvara landslide (Dolomites, Italy) and itsrelevance for hazardassessment. Geomorphology 66:149–165

Cruden DM, Varnes DJ (1996) Landslide types and processes. In: Turner AK, Schuster RL (ed) Landslides: investigation and mitigation, Transportation Research Board. Special Report 247 National Academy Press, Washington D.C

Duan QY, Sorooshian S, Gupta VK (1992) Effective and efficient global optimization for conceptual rainfall-runoff models. Water Resour Res 28(4):1015–1031

Duan QY, Gupta VK, Sorooshian S (1993) Shuffled complex evolution approach for effective and efficient global minimization. J Optim Theory Appl 76 (3):501–521

Duan QY, Sorooshian S, Gupta VK (1994) Optimal use of the SCE-UA global optimization method for calibrating watershed models. J Hydrol 158:265–284

Feng XT, Chen BR, Yang C, Zhou H, Ding X (2006) Identification of visco-elastic models for rocks using genetic programming coupled with the modified particle swarm optimization algorithm. Int J Rock Mech Min Sci 43:789–801

Finsterle S (2006) Demonstration of optimization techniques for groundwater plume remediation using iTOUGH2. Environ Model Softw 22:665–680

Francois B, Tacher L, Bonnard C, Laloui L, Triguero V (2007) Numerical modelling of the hydrogeological and geomechanical behaviour of a large slope movement: the Triesenberg landslide (Liechtenstein). Can Geotech J 44(7):840–857

Gens A, Ledesma A, Alonso EE (1996) Estimation of parameters in geotechnical backanalysis—II. Application to a tunnel excavation problem. Comput Geotech 18:29–46

Guzzetti F, Cardinali M, Reichenbach P (1994) The AVI project: a bibliographical and archive inventory of landslides and floods in Italy. Environ Manag 18 (4):623–633

Hvorslev M (1949) Subsurface exploration and sampling of soils for civil engineering purposes. Report on soil sampling, U.S. waterways experiment station, Vicksburg, pp 521

Krahn J (2004) Seepage modeling with SEEP/W. GEO-SLOPE International Ltd

Ledesma A, Gens A, Alonso EE (1996a) Estimation of parameters in geotechnical backanalysis—I. Maximum likelihood approach. Comput Geotech 18(1):1–27

Ledesma A, Gens A, Alonso EE (1996b) Parameter and variance estimation in geotechnical backanalysis using prior information. Int J Numer Anal Methods Geomech 20:119–141

Levasseur S, Malecot Y, Boulon M, Flavigny E (2008) Soil parameter identification using a genetic algorithm. Int J Numer Anal Methods Geomech 32:189–213

Malecot Y, Flavigny E, Boulon M (2004) Inverse analysis of soil parameters for finite element simulation of geotechnical structures: pressuremeter test and excavation problem. In: Brinkgreve RBJ, Schad H, Schweiger HF, Willand E (eds) Proc. Symp. GeotechnicalInnovations. Verlag Glückauf, Essen, pp 659–675

Malet JP, Laigle D, Remaitre A, Maquaire O (2005) Triggering conditions and mobility of debris flows associated to complex earthflows. Geomorphology 66 (1–4):215–235

Manly BFJ (1944) Multivariate statistical methods: a primer. 3rd Edition. Chapman & Hall, CRC

Marcato G, Mantovani M, Pasuto A, Tagliavini F, Silvano S, Zabuski L (2009) Assessing the possible future development of the Tessina landslide using numerical modelling. In: Malet JP, Remaitre A, Bogaard T (eds) Landslide processes: from geomorphological mapping to dynamic modelling. CERG, Strasbourg, France, pp 327–334

Marcato G, Mantovani M, Pasuto A, Zabuski L, Borgatti L (2012) Monitoring, numerical modelling and hazard mitigation of the Moscardo landslide (Eastern Italian Alps). Eng Geol 128:95–107

Meier J (2008) Parameterbestimmung mittels inverser Verfahren für geotechnische Problemstellungen. Dissertation.Bauhaus-Universität Weimar, Germany

Meier J, Rudolph S, Schanz T (2006) Effektiver Algorithmus zur Lösung von inversen Aufgabenstellungen. Bautechnik 83(7):470–481

Meier J, Schädler W, Borgatti L, Corsini A, Schanz T (2008) Inverse parameter identification technique using PSO algorithm applied to geotechnical modeling. Journal of Artificial Evolution and Applications, Article ID 574613, 14 pages, doi:10.1155/2008/574613

Mesri G, Castro A (1987) C_α/C_C concept and K_0 during secondary compression. J Geotech Eng 112(3):230–247

Mesri G, Godlewski P (1977) Time- and stress-compressibility interrelationship. J Geotech Eng Div 103:417–430

Panizza M, Silvano S, Corsini A, Soldati M, Marchetti M, Borgatti L, Ghinoi A, Piacentini D, Pasuto A, Zannoni A, Marcato G, Mantovani M, Tagliavini F, Moretto S (2006) Definizione della pericolosità e di possibili interventi di mitigazione della frana di Corvara in Badia. Provincia Autonoma di Bolzano, Südtirol. http://www.provinz.bz.it/wasserschutzbauten/download/Download_Corvara_RelazioneFinale_10-4-06_inviato.pdf (Accessed 18 Apr 2014)

Picarelli L, Russo C, Urciuoli G (1995) Modelling earthflow movement based on experiences. In: Danish Geotechnical Society (ed) Proceedings of the 11th European conference on soil mechanics and foundation engineering, Copenhagen, 6:157–162

Picarelli L, Di Maio C, Olivares L, Urciuoli G (2000) Properties and behaviour of tectonized clay shales in Italy. Keynote lecture, Proc. II Int. Symposium on Hard Soils and Soft Rocks, Napoli, Italy 1998, Balkema, Rotterdam, 1211–1242

PLAXIS V8 (2003) Reference manual. In: Brinkgreve RBJ (in cooperation with: Al-Khoury R, Bakker KJ, Bonnier PG, Brand PJW, Broere W, Burd HJ, Soltys G, Vermeer PA, Vogt-Breier C, Waterman D, Den Haag DOC. Technical University of Delft and PLAXIS BV, The Netherlands

Schädler W (2008) Slope movements of the earthflow type—engineering-geological investigation, geotechnical assessment and modelling of the source areas on the basis of case studies from the Alps and Apennines. Dissertation at Friedrich-Alexander-Universität Erlangen-Nürnberg. Logos Verlag Berlin GmbH, pp 212

Schanz T, Meier J (2008) Gestaltung, Validierung und Optimierung von Messprogrammen fur geotechnische Aufgabenstellungen. Bautechnik 85(5):307–316

Schanz T, Zimmerer MM, Datcheva M, Meier J (2006) Identification of constitutive parameters for numerical models via inverse approach. Felsbaumagazin 24 (2):11–21

Schwarz S (2001) Sensitivitäts analyse und Optimierung bei nicht linearen Strukturverhalten. Institute fürBaustatik, Universität Stuttgart, Bericht 34

Soldati M, Corsini A, Pasuto A (2004) Landslides and climate change in the Italian Dolomites since the Late Glacial. Catena 55:141–161

Tacher L, Bonnard C, Laloui L, Parriaux A (2005) Modelling the behaviour of a large landslide with respect to hydrogeological and geomechanical parameter heterogeneity. Landslides 2(1):3–14

Thornthwaite CW (1948) An approach toward a rational classification of climate. Geogr Rev 38:55–94

Trigila A, Iadanza C, Spizzichino D (2010) Quality assessment of the Italian Landslide Inventory using GIS processing. Landslides 7(4):455–470

van Asch T, van Beek LPH, Bogaard TA (2007) Problems in predicting the mobility of slow-moving landslides. Eng Geol 91:46–55

Vermeer PA, Neher HP (1999) A soft soil model that accounts for creep. In: Proceedings of the International Symposium (ed) Beyond 2000 in Computational Geotechnics—10 Years of PLAXIS International. Balkema, Amsterdam, pp 249–261

Vulliet L, Bonnard C (1996) The Chlöwena landslide: prediction with a viscous model. In VIIth Int. Symp. on landslides. Trondheim 1:397–402

Zhang ZF, Ward AL, Gee GW (2003) Estimating soil hydraulic parameters of a field drainage experiment using inverse techniques. Vadose Zone J 2:201–211

W. Schädler
WPW Geoconsult Südwest GmbH,
Erzbergerstraße 19, 68165 Mannheim, Germany Q1

L. Borgatti (✉)
Department of Civil, Chemical, Environmental and Materials Engineering DICAM~~, ALMA MATER STUDIORUM,~~
University of Bologna,
Viale Risorgimento 2, 40136 Bologna, Italy
e-mail: lisa.borgatti@unibo.it

A. Corsini · F. Ronchetti
Department of Chemical and Geological Sciences DSCG,
University of Modena and Reggio Emilia,
Largo Sant'Eufemia 19, 41121 Modena, Italy

J. Meier
Gruner AG,
Gellertstrasse 55, 4020 Basel, Switzerland

T. Schanz
Foundation Engineering, Soil and Rock Mechanics, Faculty of Civil and Environmental Engineering,
Ruhr-Universität Bochum,
Building IC 5, Universitätsstrasse 150, 44780 Bochum, Germany

AUTHOR QUERIES

AUTHOR PLEASE ANSWER ALL QUERIES.

Q1. Please check if affiliations are presented correctly.
Q2. Please indicate the significance of the asterisk in Table 5.
Q3. Please check Tables 1-8 if captured and presented correctly.